Spin Susceptibility above the Superfluid Onset in Ultracold Fermi Gases

Yun Long⬤, Feng Xiong, and Colin V. Parker⬤*
School of Physics, Georgia Institute of Technology, Atlanta, Georgia 30332, USA

Ultracold atomic Fermi gases can be tuned to interact strongly, which produces a display of spectroscopic signatures above the superfluid transition reminiscent of the pseudogap in cuprates. However, the extent of the analogy can be questioned since many thermodynamic quantities in the low temperature spin-imbalanced normal state can be described successfully using Fermi liquid theory. Here we present spin susceptibility measurements across the interaction strength-temperature phase diagram using a novel radio frequency technique with ultracold ^{6}Li gases. For all significant interaction strengths and at all temperatures we find the spin susceptibility is reduced compared to the equivalent value for a noninteracting Fermi gas. At unitarity, we can use the local density approximation to extract the integrated spin susceptibility for the uniform gas as a function of temperature, which at high temperatures is generally less than theoretically predicted. At low temperatures, our data lie within the range of theoretical predictions, although we can also describe the entire curve using a very simple one-parameter mean field model with monotonically increasing spin susceptibility.

In the study of strongly interacting quantum systems, the Bose-Einstein condensation–Bardeen-Cooper-Schrieffer (BEC-BCS) crossover is a simple and experimentally realizable model [1–3] with implications for a variety of physical systems such as the high-T_c cuprates [4] and neutron matter [5,6]. In this model, a two-component Fermi gas has an attractive contact interaction of varying strength. When the interaction is weak, the BCS state forms, while for strong interactions the fermions form composite (bosonic) molecules, which then condense into a BEC. The crossover occurs as these two states connect to one another by tuning the interaction strength, parameterized by $(k_F a)^{-1}$, where k_F is the Fermi wave vector and a is the s-wave scattering length. A fundamental question that emerges from this model is the degree to which it embodies something universal about strongly interacting fermions, that is, which strongly interacting fermionic systems can be approximately mapped to an effective theory falling somewhere along the crossover. In particular, for the cuprates, the phenomenon of the depressed density of states above the transition temperature known as the pseudogap [7,8] has been suggested to be due to a "preformed pairs" state analogous to the BEC-BCS crossover [4]. Although one does not expect the complete, complex phenomenology of cuprates in the BEC-BCS crossover, it remains an open question whether the cuprate pseudogap derives fundamentally from a strongly interacting pairing mechanism. If so, one would expect an analog pseudogap in ultracold gases.

In light of these possible similarities, an important project is to compare the measured properties between ultracold gases at the BEC-BCS crossover to their equivalent in materials. For spectroscopic properties, one can compare the angle-resolved photoemission spectroscopy measurements of the cuprates [7,9–11] to their ultracold gas analogs [12–14]. However, one expects the spectroscopic measurements to be strongly influenced by the nature of the particles' dispersion curve, which is parabolic for ultracold gases but significantly not so in materials [15], which in addition can have surface effects. In cold gases, spectroscopy from uniform samples [16] has also shown evidence of non-Fermi-liquid behavior. Bulk thermodynamic measurements [17–19] are an alternative, as they can be deduced from the equation of state (EoS) of a trapped atomic gas [20–25]. An appealing property for comparisons is the spin susceptibility. This property is easily calculated for the noninteracting Fermi gas, which provides a natural scale and is directly measurable in materials—for example, using the NMR Knight shift [26,27]. In NMR measurements of cuprates, a clear decrease of the spin susceptibility is observed below the pseudogap onset temperature T^*. Although a reduction of spin susceptibility can be caused by many factors, in the cuprates it is associated with a reduction in the density of states at the Fermi energy, which has been confirmed to exist based on many other measurements [7].

In ultracold Fermi gases, the situation is less clear: some theoretical calculations of the spin susceptibility have predicted a weak temperature dependence (except possibly close to the transition temperature) and a generally mean field form [28–32], while others have found significant temperature dependence over a large temperature range closer to that seen in cuprates [33]. In experiments with Fermi gases, the spin susceptibility has been determined from the EoS [34] from out-of-equilibrium dynamics [19,35]

and measured using speckle-field imaging [36]. These studies found that the spin susceptibility near the onset of superfluidity is significantly reduced from the expected value for a noninteracting gas but did not establish the temperature dependence. Therefore, such reductions are consistent with any combination of a temperature-independent mean field reduction due to interactions and a more exotic situation involving a reduction in the susceptibility below a specific T^*. The latter scenario would be predicted by any model with a strong spin-singlet gap reducing the density of states with decreasing temperature. Here we present the first comprehensive study of spin susceptibility over the entire interaction strength-temperature phase diagram, showing that for interaction strengths near unitarity the spin susceptibility is suppressed significantly even at elevated temperatures. This indicates that any reduction in susceptibility, starting from our measured value at high temperatures, would necessarily lead to a very small residual susceptibility at the superfluid onset with respect to that of a noninteracting Fermi gas at the same temperature.

We developed a novel method to measure the spin susceptibility by radio frequency (rf) dressing. With a resonant rf driving between two hyperfine states, in the interaction picture, a chemical potential difference $\Delta\mu = \mu_+ - \mu_- = \hbar\Omega$ between the two dressed states is created, where $\Omega/(2\pi)$ is the Rabi frequency. This can be thought of as an effective Zeeman field, and we can extract the susceptibility from the dressed states' number difference after equilibrium is reached. Labeling the hyperfine ground states of ^{6}Li with $|1\rangle$ from the bottom, we use a mixture of states $|2\rangle$ and $|3\rangle$, which are adiabatically connected to the $|m_J, m_I\rangle = |-1/2, 0\rangle$ and $|-1/2, -1\rangle$ states in the high field limit or $|F, m_F\rangle = |1/2, -1/2\rangle$ and $|3/2, -3/2\rangle$ in the low field limit, respectively. We begin by preparing this mixture using standard ultracold atom methods, yielding a Fermi gas with 2×10^4 to 1×10^5 atoms in each pin state at temperatures ranging from several times T_F^t down to $0.15 \cdot T_F^t$ [37], where $T_F^t = E_F^t/k_B = \hbar(\omega_x\omega_y\omega_z)^{1/3}(3N)^{1/3}/k_B$ is the trap Fermi temperature and $\omega_i/(2\pi), (i = x, y, z)$ are the trap frequencies. In our experiments, the trap Fermi energy E_F^t ranges from 12 to 55$h \cdot$ kHz. The initial mixture is spin imbalanced with a typical majority:minority ratio of $2:1$, and the gas is held in a single-beam optical trap, with confinement along the beam axis provided by the magnetic field. Typical trapping frequencies are $2\pi \times 30$ Hz along the beam axis and $2\pi \times 1$–2 kHz in the perpendicular directions. We then expose the gas to rf radiation on the $|2\rangle \Leftrightarrow |3\rangle$ transition. The radiation is initially $2\pi \times 100$ kHz detuned and then adiabatically ramped onto resonance in 47 ms, mapping the spin imbalance from the initial basis of $|2\rangle$ and $|3\rangle$ states into an imbalance in the rf-dressed basis, which we denote by $|+\rangle$ and $|-\rangle$. In the rotating wave approximation, these states have energies of $+\hbar\Omega/2$ and $-\hbar\Omega/2$, respectively. In our experiment, $\Omega = 2\pi \times 1.4$ kHz, which is small

compared to other energy scales and gives a linear response [37]. Once the rf radiation is on resonance, we allow the sample to reach equilibrium for a holding time of typically 2 s. The gas is held in a magnetic field gradient, which provides a large scalar force together with a small spin-dependent force. The spin-dependent force is small (of the order nK/μm) because the magnetic moment of the two states is very nearly equal. However, the spin-dependent potential gradient associated with this force is sufficient to allow the dressed state populations to exchange and reach thermodynamic equilibrium [37]. Following the hold period, we adiabatically ramp the radiation to a $2\pi \times 100$ kHz detuning, which maps the imbalance back into the $|2\rangle - |3\rangle$ basis, where we image the sample in situ using phase-contrast imaging.

We choose the sign of the initial and final detuning in a specific way to avoid possible bias from slight imaging frequency offsets and/or residual initial spin imbalance. We perform the experiment with all four possible signs of initial and final detuning, using otherwise identical procedures. To simplify the description, we use "R" and "B" to denote initial or final detuning, which is negative (red) or positive (blue). Thus, a "BB" experiment consists of ramping the rf frequency from above resonance onto the resonance, holding for 2 s, and ramping again to a higher frequency. Phase-contrast images of the differential spin density from a typical experimental run after applying our enhanced principle component algorithm [41] are shown in Figs. 1(a)–1(d), with a positive signal corresponding to an
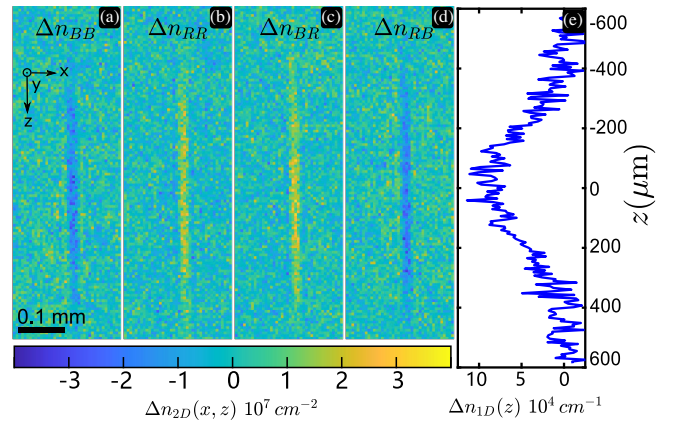

FIG. 1. Four closely related experiments with the same atomic cloud preparation but different rf procedures. (a)–(d) The first (second) subscript character on Δn denotes the direction of an adiabatic sweep onto (away from) resonance, where B (R) represents blue (red) detuning. We hold the rf for 2 s on resonance between the sweeps. The rf procedure generates a spin difference leading to positive signal in (b) and (c) and negative signal in (a) and (d). (e) 1D profile along the z axis of the trap from summing the net differential signal $(-\Delta n_{BB} + \Delta n_{RR} + \Delta n_{BR} - \Delta n_{RB})/4$ over the x direction with a 29 μm wide region centered on the atomic cloud. The data comes from a unitary gas at 210 nK ($T/T_F^t = 0.27$).

excess density of state $|2\rangle$. The quantities $-\Delta n_{BB} + \Delta n_{RR}$ and $\Delta n_{BR} - \Delta n_{RB}$ are insensitive to any hypothetical initial imbalances that persist through the experiment, since BB/RR and BR/RB are mirrored pairs from the perspective of Landau-Zener sweeps, which respectively leave the spin population unchanged and invert the imbalance, in the limit of no relaxation. Similarly $-\Delta n_{BB} + \Delta n_{BR}$ and $\Delta n_{RR} - \Delta n_{RB}$ are insensitive to imaging offset because the dressed spin imbalance prior to the final ramp is mapped onto opposite final states. Hence the quantity $\Delta n = (-\Delta n_{BB} + \Delta n_{RR} + \Delta n_{BR} - \Delta n_{RB})/4$ corrects for both possibilities. Figure 1(e) shows the row-summed differential signal generated by our rf method. These data will form the basis for our analysis. It is worth noting that our method for generating the imbalance is distinct from our imaging method [37] and that therefore any method of spin-selective imaging could be employed, such as a quantum gas microscope, magneto-optical trap recapture, or resonant ionization detection.

By calibrating with the total atom number in each spin state, we can determine the long axis differential axial density profile $\Delta n_{1D}(z)$. We define an orthogonal coordinate system where $\hat{z}$ runs along the trapping beam axis, $\hat{y}$ is in the direction opposing gravity and colinear with the magnetic field and the magnetic gradient, and $\hat{x}$ is the remaining direction. The axial density therefore represents the density integrated over x and y. We present this for a weakly interacting gas and a unitary gas in Fig. 2 in the scaled form $\Delta n_{1D}(z) \cdot R_F/N$, where N is the total atomic number and $R_F = \sqrt{2E_F^t/[m(\omega_x\omega_y\omega_z)^{2/3}]}$ is the Thomas-Fermi radius. For comparison to theoretical models, we acquire the long axis total axial density profile $n_{1D}(z)$ and use this information together with the local density approximation and a published EoS measurement at

FIG. 2. Differential column density measured at (a) 40.0 mT where interaction is close to zero at 513 nK ($T/T_F^t = 0.63$) and (b) 81.4 mT near the unitary point at 210 nK ($T/T_F^t = 0.27$). The red dashed lines in (a) and (b) show the noninteracting susceptibility for a gas with the same density profile. In (b), the black solid line is from our mean field model.

unitarity [39] to determine the three-dimensional density profile and temperature in our trap. Away from unitarity, we use a phenomenological fit based on a polylogarithm, which yields similar results [37]. From the density profile, we can compute the expected spin difference from a susceptibility model and integrate to generate the expected spin difference. We do this for two models, the ideal Fermi gas model, which describes the weakly interacting data well but not the unitary data, and the mean field model described below.

We model the spin susceptibility of the system, which is given by

$$\chi^{-1} = \partial H/\partial M = (\partial^2 F/\partial M^2)_{T,V,N}, \quad (1)$$

where F is the Helmholtz free energy of the system, $H = \mu_\uparrow - \mu_\downarrow$ is the analog of the magnetic field, and $M = N_\uparrow - N_\downarrow$ is the magnetization. In a mean field picture, the interaction simply adds a temperature-independent term $F_I = \alpha M^2/(2\chi_{NI}^0)$ to the free energy, where χ_{NI}^0 is the noninteracting susceptibility at zero temperature (in Fermi-liquid theory α is proportional to the parameter F_0^a). A more complete Fermi-liquid theory would also add an effective mass, but the effective mass correction is small for strongly interacting Fermi gases [34]. This then results in a susceptibility $\chi^{-1}(T) = \chi_{NI}^{-1}(T) + \alpha\chi_{NI}^0{}^{-1}$, where $\chi_{NI}(T)$ is the noninteracting spin susceptibility at temperature T.

At unitarity, where the entire trap has the same interaction parameter, we can scale the data into a dimensionless form that is independent of trapping conditions and use the local density approximation to express our measurement purely in terms of the local properties of a uniform gas. In particular, we consider the dimensionless integrated susceptibility given by

$$\bar{\chi} = \int_{-\infty}^{\mu} \chi(\mu')\lambda_{dB}^3 d\mu', \quad (2)$$

where $\lambda_{dB} = \sqrt{2\pi\hbar^2/(mk_BT)}$ is the thermal de Broglie wavelength. This is shown in Fig. 3. For lower temperature samples, at the center of the trap the data shows a plateau (blue points in Fig. 3). This is expected for a superfluid for which the spin susceptibility has vanished. Indeed, the onset occurs where the local $T/T_F = 0.19$, below a theoretical estimate [42] but slightly above other experiments [43,44]. The onset is determined by performing a best fit between our data and the mean field model. When the sample is partially superfluid, there are significant parasitic effects that tend to balance the spins as the sample evaporates, meaning that the absolute calibration of susceptibility is no longer possible and the calibration has to be done based on overlap with totally nonsuperfluid samples [37]. Taking all the unitary data together, over a large range of temperatures down to the superfluid transition, we see a significant reduction compared to
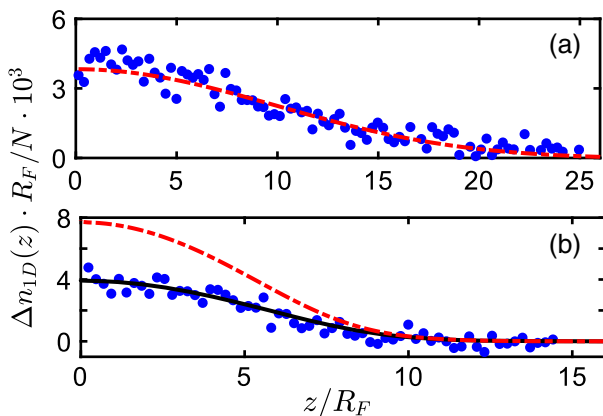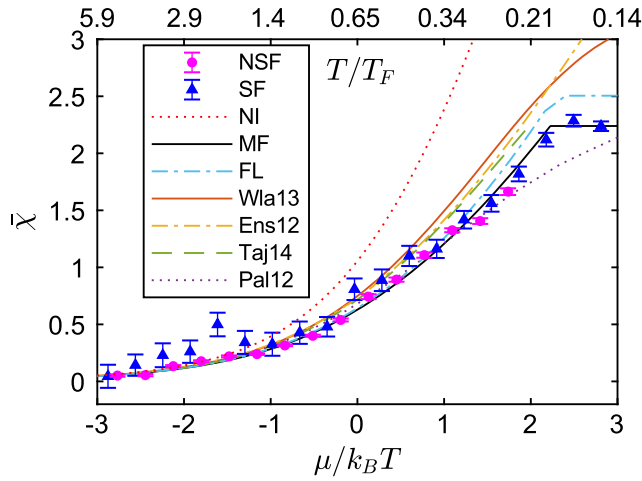
FIG. 3. Dimensionless integrated susceptibility $\bar{\chi}$. The acronyms "NSF" and "SF" stand, respectively, for experimental data with all nonsuperfluid and with superfluid at the center of the trap; "NI" is the noninteracting Fermi gas result, "MF" is our mean field model with $\alpha = 1.61$. "Wla13," "Ens12," "Taj14," and "Pal12" are theoretical results extracted from Refs. [28,29,32,33], respectively, while "FL" is a Fermi liquid model extracted from Ref. [32]. Error bars are derived from the standard deviation of the measurements.
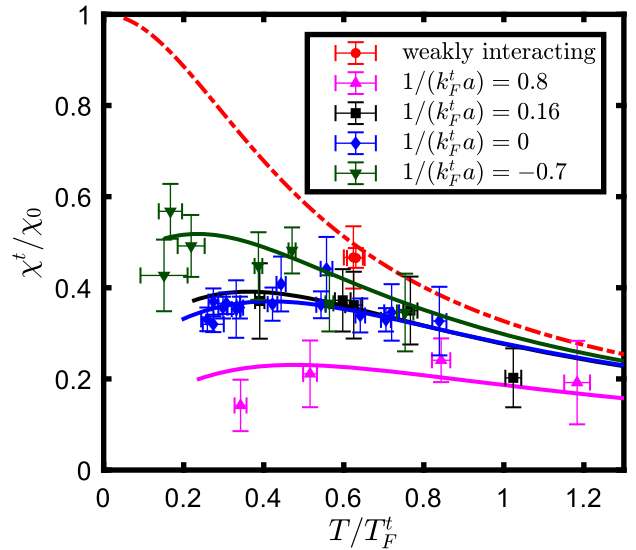

FIG. 4. The trap-averaged spin susceptibility normalized to the zero-temperature noninteracting value for weak interactions and across the BEC-BCS crossover. The red dotted line shows the susceptibility of a noninteracting Fermi gas as a function of temperature. Error bars are derived from the standard deviation of many shots (for susceptibility) and from fitting uncertainty (for temperature). Solid curves are calculated using the measured density distribution and our mean field model under the local density approximation, with values of the fit parameter α given by 3.5, 1.5, 1.6, and 0.9 from top to bottom.

the noninteracting expectation. However, we are able to describe this reduction over the whole temperature range using the mean field model. For comparison, we have included integrated susceptibilities extracted from several published results for the spin susceptibility. The measured value is closest to the Fermi liquid calculation, and it is less than the predictions with the exception of Ref. [33], which is smaller than the measurement at the lowest temperatures. Our key result is that the susceptibility is suppressed substantially from the noninteracting value at high temperature (well above T_c and into the region where $\mu < 0$), typically more than theories have predicted. Since among the theoretical calculations, those featuring stronger temperature dependence predict higher susceptibilities in this temperature range, our measurement favors those models with little temperature dependence, such as the Fermi liquid theory (taken from Ref. [32]) or the calculations in Refs. [28,29]. The exception is Ref. [33], whose prediction is in fact below the data near the superfluid phase despite being above it in the higher temperature range. This is consistent with there being less decrease of susceptibility with temperature than predicted in Ref. [33]. Details of how we compare these models are presented in the Supplemental Material [37].

In order to evaluate the susceptibility away from unitarity, we have performed these measurements throughout the phase diagram of the BEC-BCS crossover. Figure 4 summarizes our main result from this perspective. We show trap-averaged measurements of the spin

susceptibility, normalized to the value for a trapped noninteracting gas with the same atom number at zero temperature (to facilitate comparison to Ref. [45]). We characterize the temperature by the ratio T/T_F^t. Similarly, we characterize the interaction strength as $(k_F^t a)^{-1}$, where $k_F^t = (2mk_BT_F^t)^{1/2}$. The solid curves are calculated with our mean field model and take into account the experimental density profiles, which leads to slight nonmonotonic behavior for trap-averaged susceptibility [45]. The mean field model continues to agree well with our data throughout the phase diagram (a different mean field parameter is used for each value of the interaction strength). Consistent with previous results [36] and theory [28,45], we find the trap-averaged susceptibility at the onset of superfluidity to be about $33 \pm 3\%$ of the noninteracting value when $(k_F a)^{-1} = 0$. Extrapolating our model to the lowest temperatures, the susceptibility ratio with a uniform noninteracting gas would be $38 \pm 1\%$, slightly less than the value of approximately 50% for a model calibrated to data extrapolated from spin-imbalanced samples at low temperatures [34]. The uncertainty in these figures is purely statistical, while any of the foreseeable systematic effects would come from parasitic equilibration or insufficient equilibration time and cause the measured susceptibility to be too low. We believe the systematic effects are no larger than 10% of the measured signal, so 4% of the

noninteracting value [37]. Further to the BEC side, where $(k_F^t a)^{-1} = 0.8$, the susceptibility is drastically reduced at all temperatures.

In conclusion, we surveyed the spin susceptibility of strongly interacting ^{6}Li gases from the BCS side to the BEC side and from high temperatures down to the superfluid transition temperature. The temperature dependence of the spin susceptibility can be modeled reasonably throughout the phase diagram using a mean field model. Compared to theoretical calculations, the data show in general a lower susceptibility, particular at temperatures above $0.5 \cdot T_F$. We extracted results for the integrated susceptibility of a uniform gas. The integration makes precise statements about the behavior immediately above the transition difficult, but coupled with other measurements [34,36] our high-temperature results leave little room for a sharp decrease in susceptibility with reducing temperatures. Future experiments could likely reduce the uncertainty considerably by increasing the fraction of imaging photons captured, and planned experiments imaging uniform density regions rather than integrating along the imaging axis could resolve the region just above T_c more easily. The closest analogy to a strong decrease of spin susceptibility with temperature in the BEC-BCS crossover of ultracold Fermi gases is the far BEC side, where there may be a significant percentage reduction in the already small susceptibility at 1.5–2 times T_c, and of course pairing above the transition is expected in this range. All of this sits in contrast to spectroscopic evidence showing that even on the near BEC side coherent excitations are absent, meaning that coherence is lost before the temperature dependence of the susceptibility deviates significantly from mean field form. This presents a challenge to "general theories" of pseudogap [8], since these two phenomena would need to occur in the same order with respect to changes of the system parameters (e.g., interaction strength, doping) across the various systems where such a theory might be applied. Finally, we mention that the method we introduced to measure the susceptibility is versatile and can be feasibly extended to various ultracold atom systems—for example, spinor Bose gases, 2D gases, or gases within optical lattices.

*cparker@gatech.edu

[1] P. Nozires and S. Schmitt-Rink, J. Low Temp. Phys. **59**, 195 (1985).

[2] S. Giorgini, L. P. Pitaevskii, and S. Stringari, Rev. Mod. Phys. **80**, 1215 (2008).

[3] M. Randeria and E. Taylor, Annu. Rev. Condens. Matter Phys. **5**, 209 (2014).

[4] Q. Chen, J. Stajic, S. Tan, and K. Levin, Phys. Rep. **412**, 1 (2005).

[5] J. Margueron, H. Sagawa, and K. Hagino, Phys. Rev. C **76**, 064316 (2007).

[6] G. C. Strinati, P. Pieri, G. Rpke, P. Schuck, and M. Urban, Phys. Rep. **738**, 1 (2018).

[7] T. Timusk and B. Statt, Rep. Prog. Phys. **62**, 61 (1999).

[8] E. J. Mueller, Rep. Prog. Phys. **80**, 104401 (2017).

[9] H. Ding, T. Yokoya, J. C. Campuzano, T. Takahashi, M. Randeria, M. R. Normant, T. Mochikull, K. Kadowaki, and J. Giapintzakis, Nature (London) **382**, 51 (1996).

[10] A. Damascelli, Z. Hussain, and Z.-X. Shen, Rev. Mod. Phys. **75**, 473 (2003).

[11] I. M. Vishik, Rep. Prog. Phys. **81**, 062501 (2018).

[12] J. T. Stewart, J. P. Gaebler, and D. S. Jin, Nature (London) **454**, 744 (2008).

[13] J. Gaebler, J. Stewart, T. Drake, D. Jin, A. Perali, P. Pieri, and G. Strinati, Nat. Phys. **6**, 569 (2010).

[14] Y. Sagi, T. E. Drake, R. Paudel, R. Chapurin, and D. S. Jin, Phys. Rev. Lett. **114**, 075301 (2015).

[15] M. R. Norman, M. Randeria, H. Ding, and J. C. Campuzano, Phys. Rev. B **52**, 615 (1995).

[16] B. Mukherjee, P. B. Patel, Z. Yan, R. J. Fletcher, J. Struck, and M. W. Zwierlein, Phys. Rev. Lett. **122**, 203402 (2019).

[17] L. Luo, B. Clancy, J. Joseph, J. Kinast, and J. E. Thomas, Phys. Rev. Lett. **98**, 080402 (2007).

[18] T.-L. Ho, Phys. Rev. Lett. **92**, 090402 (2004).

[19] G. Valtolina, F. Scazza, A. Amico, A. Burchianti, A. Recati, T. Enss, M. Inguscio, M. Zaccanti, and G. Roati, Nat. Phys. **13**, 704 (2017).

[20] M. W. Zwierlein, C. H. Schunck, A. Schirotzek, and W. Ketterle, Nature (London) **442**, 54 (2006).

[21] F. Chevy, Phys. Rev. A **74**, 063628 (2006).

[22] Y. I. Shin, C. H. Schunck, A. Schirotzek, and W. Ketterle, Nature (London) **451**, 689 (2008).

[23] Y. I. Shin, Phys. Rev. A **77**, 041603 (2008).

[24] S. Nascimbene, N. Navon, K. J. Jiang, F. Chevy, and C. Salomon, Nature (London) **463**, 1057 (2010).

[25] N. Navon, S. Nascimbene, F. Chevy, and C. Salomon, Science **328**, 729 (2010).

[26] R. E. Walstedt, W. W. Warren, R. F. Bell, R. J. Cava, G. P. Espinosa, L. F. Schneemeyer, and J. V. Waszczak, Phys. Rev. B **41**, 9574 (1990).

[27] M. Takigawa, A. P. Reyes, P. C. Hammel, J. D. Thompson, R. H. Heffner, Z. Fisk, and K. C. Ott, Phys. Rev. B **43**, 247 (1991).

[28] H. Tajima, T. Kashimura, R. Hanai, R. Watanabe, and Y. Ohashi, Phys. Rev. A **89**, 033617 (2014).

[29] T. Enss and R. Haussmann, Phys. Rev. Lett. **109**, 195303 (2012).

[30] S. Jensen, C. N. Gilbreth, and Y. Alhassid, Eur. Phys. J. Special Topics **227**, 2241 (2019).

[31] A. Richie-Halford, J. E. Drut, and A. Bulgac, Phys. Rev. Lett. **125**, 060403 (2020).

[32] G. Wlazlowski, P. Magierski, J. E. Drut, A. Bulgac, and K. J. Roche, Phys. Rev. Lett. **110**, 090401 (2013).

[33] F. Palestini, P. Pieri, and G. C. Strinati, Phys. Rev. Lett. **108**, 080401 (2012).

[34] S. Nascimbene, N. Navon, S. Pilati, F. Chevy, S. Giorgini, A. Georges, and C. Salomon, Phys. Rev. Lett. **106**, 215303 (2011).

[35] A. Sommer, M. Ku, G. Roati, and M. W. Zwierlein, Nature (London) **472**, 201 (2011).

[36] C. Sanner, E. J. Su, A. Keshet, W. Huang, J. Gillen, R. Gommers, and W. Ketterle, Phys. Rev. Lett. **106**, 010402 (2011).

[37] See Supplemental Material at http://link.aps.org/supplemental/10.1103/PhysRevLett.126.153402, which includes the following sections: "Preparation of atomic clouds" (including Ref. [38]); "Imaging and calibration"; "Density profile imaging"; "Harmonic trap approximation"; "Extraction of the 3D density profile" (including Ref. [39]); "Temperature determination" (including Ref. [40]); "Equilibration time and linearity"; "Parasitic evaporative effects"; "Theoretical modeling of the spin-imbalancing process"; and "Mean field fitting and theory comparison" (including Ref. [28], [29], [32], and [33]).

[38] Y. Long, F. Xiong, V. Gaire, C. Caligan, and C. V. Parker, Phys. Rev. A **98**, 043626 (2018).

[39] T.-L. Ho and Q. Zhou, Nat. Phys. **6**, 131 (2010).

[40] M. J. H. Ku, A. T. Sommer, L. W. Cheuk, and M. W. Zwierlein, Science **335**, 563 (2012).

[41] F. Xiong, Y. Long, and C. V. Parker, J. Opt. Soc. Am. B **37**, 2041 (2020).

[42] A. Perali, P. Pieri, L. Pisani, and G. C. Strinati, Phys. Rev. Lett. **92**, 220404 (2004).

[43] E. Burovski, E. Kozik, N. Prokofev, B. Svistunov, and M. Troyer, Phys. Rev. Lett. **101**, 090402 (2008).

[44] P. Magierski, G. Wlazlowski, and A. Bulgac, Phys. Rev. Lett. **107**, 145304 (2011).

[45] H. Tajima, R. Hanai, and Y. Ohashi, Phys. Rev. A **96**, 033614 (2017).